Atomic and macroscopic measurements of attosecond pulse trains

Dahlström, Marcus; Fordell, Thomas; Mansten, Erik; Ruchon, T.; Swoboda, Marko; Klünder, Kathrin; Gisselbrecht, Mathieu; L'Huillier, Anne; Mauritsson, Johan

Published in:
Physical Review A (Atomic, Molecular and Optical Physics)

DOI:
10.1103/PhysRevA.80.033836

2009

Atomic and macroscopic measurements of attosecond pulse trains

J. M. Dahlström[1], T. Fordell[1], E. Mansten[1], T. Ruchon[2],
M. Swoboda[1], K. Klünder[1], M. Gisselbrecht[1,3], A. L'Huillier[1], J. Mauritsson[1]
[1] *Department of Physics, Lund University, P.O. Box 118, SE-221 00 Lund, Sweden*
[2] *CEA-Saclay, DSM, Service des Photons, Atomes et Molcules, 91191 Gif sur Yvette, France*
[3] *CNRS-Université Paris Sud, UMR8624, LIXAM, Bat. 350, 91405, Orsay, France*

We characterize attosecond pulses in a train using both the well established "Reconstruction of Attosecond Beating by Interference of Two Photon Transitions" (RABITT) technique and the recently demonstrated *in-situ* method, which is based on a weak perturbation of the harmonic generation process by the second harmonic of the laser field. The latter technique determines the characteristics of the single atom emission, while RABITT allows one to measure attosecond pulses "on target". By comparing the results of the two methods, the influence of propagation and filtering on the attosecond pulses can be extracted.

PACS numbers: 32.80.Rm, 32.80.Qk, 42.65.Ky

I. INTRODUCTION

Attosecond pulse trains (APTs) are created when intense infrared (IR) laser pulses interact with a gas of atoms or molecules [1]. The characteristics of the attosecond pulses depend both on the quantum-mechanical single atom dynamics as well as on macroscopic effects due to propagation in the nonlinear medium [2]. Under normal experimental conditions, the pulse train contains two pulses per cycle of the laser field [3–5]. The properties of these pulses can be modified by transmission through filters [6] or reflection by gratings and/or multilayer mirrors [7]. Several techniques to characterize attosecond pulse trains have been proposed, each with specific advantages and limitations. In this paper we concentrate on analyzing and comparing two of these techniques: the Reconstruction of Attosecond Beating by Interference of Two-photon Transitions (RABITT) [1] and a two-color *in-situ* method [8], that uses a weak perturbation of high order harmonic generation (HHG) by the second harmonic of the fundamental laser field. Both techniques aim to characterize the average attosecond pulse structure in an APT.

Fig. 1 illustrates schematically the difference between these two techniques. RABITT allows us to determine the *final* structure of the attosecond pulses after propagation in the gas cell and filtering. The attosecond pulses are characterized "on-target", *i.e.*, in the chamber where they can be used for applications. The RABITT scheme is implemented by ionizing an atomic gas with the APT in presence of a synchronized weak IR field. The perturbation due to the IR field results in sidebands in the photoelectron spectra as shown in Fig. 2(a). Information about the structure of the attosecond pulses can then be obtained by studying the intensity oscillations of these sidebands with respect to the subcycle delay between the probe field and the APT.

The *in-situ* method measures the single atom emission from the individual atoms. In contrast to RABITT, the *initial* shape of the attosecond pulses, before propagation and filtering, is now measured [Fig. 1]. This is important for applications that are conducted in the generation process itself, *e.g.* the tomography of electronic orbitals [9]. The presence of a weak second harmonic (blue) field in the generation chamber leads to the generation of even harmonics as shown in Fig. 2(b) [10]. The harmonic generation process is nonlinear beyond the perturbative regime, which results in comparable probabilities for the processes shown in Fig. 2(b) even though the number of IR photons absorbed differs by four. Information about the initial properties of the attosecond pulse is obtained by studying the intensity oscillations of the even harmonics with respect to the phase between the IR and the blue field.

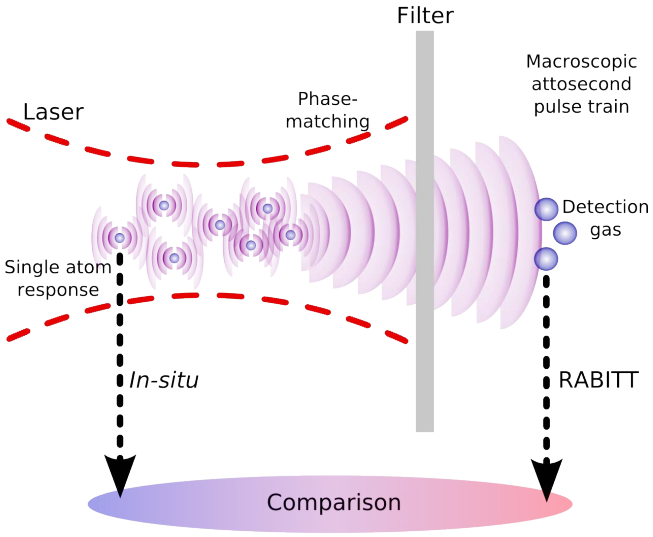

FIG. 1: (Color online) Cartoon illustrating the differences between the two characterization methods. The *in-situ* method measures the single atom emission, while the RABITT scheme determines the corresponding attosecond pulses "on-target". The influence of phase matching and filtering on the attosecond pulses can be deduced through the implementation of both methods on the same HHG set-up.

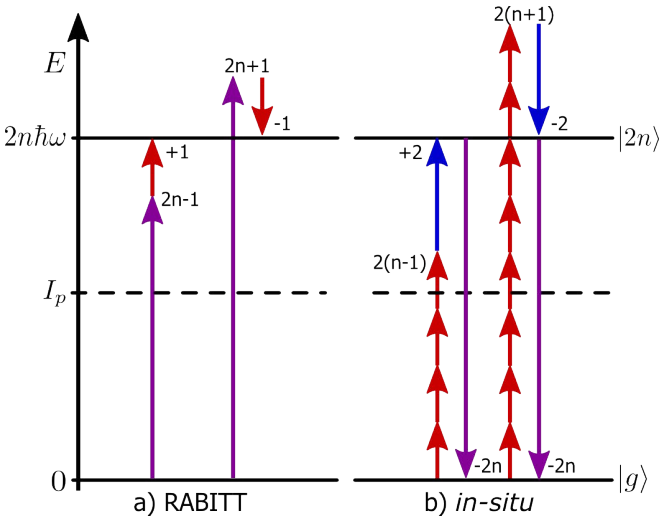

FIG. 2: (Color online) Energy diagrams associated with the two characterization methods. (a) Sidebands are created through the absorption/emission of an IR photon (ω_R) in the RABITT method. (b) Even harmonics are produced in the *in-situ* method due to the presence of a weak blue field ($2\omega_R$). Attosecond pulses are characterized by studying the interferences arising from the degenerate ways of reaching the sidebands or even harmonics.

In this paper we present a detailed theoretical and experimental comparison between the two characterization methods. Implementing both schemes allows us to measure both the initial and final shape of the attosecond pulses. From these measurements the influence of propagation as well as filtering can be determined. The paper is composed as follows: Section II reviews the theory of the two characterization methods, Section III gives an overview of the experimental setup, Section IV presents results from both methods at low gas generation pressure, Section V discusses the reasons for the difference observed at higher gas pressures and Section VI summarizes the article with an outlook.

II. THEORY

The electric field of an attosecond pulse can be written as $\tilde{E}(t) = \tilde{\Lambda}(t)\exp[i\tilde{\phi}(t)]$, where $\tilde{\Lambda}(t)$ and $\tilde{\phi}(t)$ represent the temporal envelope and phase respectively. It can also be described through its Fourier transform

$$E(\omega) = \Lambda(\omega)\exp\left[i\phi(\omega)\right] \quad (1)$$

$$= \int dt\ \tilde{\Lambda}(t)\exp\left[i\tilde{\phi}(t) - i\omega t\right], \quad (2)$$

where $\Lambda(\omega)$ and $\phi(\omega)$ are the spectral envelope and phase. The Fourier integral in Eq. 2 can be approximated using the saddle point method when the linear part in the temporal phase cancels the Fourier component,

$$\left.\frac{d\tilde{\phi}}{dt}\right|_{t=t'(\omega)} - \omega = 0, \quad (3)$$

and the quadratic part of the temporal phase is large,

$$\left.\left|\frac{d^2\tilde{\phi}}{dt^2}\right|\right|_{t=t'(\omega)} \gg 0. \quad (4)$$

Note that the temporal phase must be expanded at different times for different Fourier components, *i.e.* the saddle point time is a function of frequency, $t'(\omega)$. The saddle point approximation yields

$$E(\omega) \approx \sqrt{\frac{2\pi}{\left|\frac{d^2\tilde{\phi}}{dt^2}\right|}}\ \tilde{\Lambda}(t)\ \exp\left[i\tilde{\phi}(t) - i\omega t \pm \frac{i\pi}{4}\right]\Bigg|_{t=t'(\omega)} \quad (5)$$

where the positive (negative) phase factor corresponds to a positive (negative) chirp which is the case for attosecond pulses from the short (long) branch. The spectral phase is approximately equal to

$$\phi(\omega) = \tilde{\phi}(t'(\omega)) - \omega t'(\omega) \pm \frac{\pi}{4}, \quad (6)$$

and its first derivative is

$$\frac{d\phi}{d\omega} = -t'(\omega), \quad (7)$$

which is obtained using the chain rule and Eq. 3. We can, therefore, interpret the group delay (GD $= -d\phi/d\omega$) as the time when the temporal phase oscillates as ω. A deeper analysis is needed if Eq. 3-4 are not satisfied, which is the case of frequencies above the harmonic cutoff.

We define the relative timing of spectral components (or relative group delay) as

$$t^{(rel)}(\omega,\omega_0) = t'(\omega) - t'(\omega_0) = -\frac{d\phi}{d\omega} + \left.\frac{d\phi}{d\omega}\right|_{\omega_0} \quad (8)$$

where $t^{(rel)}(\omega,\omega_0)$ is the time is takes for the attosecond pulse to go from oscillating at ω_0 to oscillating at ω. The reference frequency, ω_0, is arbitrarily chosen to be the lowest frequency of the pulse.

In the present work performed with relatively long (multicycle) driving pulses, the emission spectrum contains peaks at harmonic frequencies. In what follows, we use the following notation for the spectral phase $\Phi_n = \phi(n\omega_R)$ where n is the harmonic number and ω_R is the angular frequency of the IR laser field.

A. RABITT

The sidebands that appear in the RABITT method can be understood through the use of second order perturbation theory [1]: absorption of a high-order harmonic

photon followed by absorption or emission of an IR photon. Interferences occur between the different quantum paths that lead to the same sideband [Fig. 2(a)]. If we assume that the competing quantum paths have the same amplitude, then the intensity of the sideband varies as

$$I_{2n}(\varphi) \propto 1 + \cos\left[2\varphi - \Delta\Phi_{2n} - \Delta\Phi_{2n}^{at}\right], \qquad (9)$$

where φ is the phase of the probe field oscillations relative to the attosecond pulses, $\Delta\Phi_{2n} = \Phi_{2n+1} - \Phi_{2n-1}$ is the difference between the phases of the corresponding harmonics and $\Delta\Phi_{2n}^{at}$ is the difference in atomic phase for the corresponding energies [11]. The atomic phase is neglected in the following because it only has a small effect on the final result in the spectral region that we consider. The first derivative of the spectral phase can then be determined using the approximate relation

$$\left.\frac{d\phi}{d\omega}\right|_{2n\omega_R} \approx \frac{\Delta\Phi_{2n}}{2\omega_R}. \qquad (10)$$

The final shape of an average attosecond pulse in the APT can be reconstructed using Eq. 10 combined with a measurement of the spectrum [12]. The aim of this paper is, however, not to reconstruct attosecond pulses but rather to study how the corresponding relative timing is affected by macroscopic dispersion in the generation cell. Using Eq. 8-10, the relative timing can be written as a function of experimental observables as

$$t_{final}^{(rel)}(\omega, \omega_0) \approx -\frac{1}{\omega_R}\left[\varphi_{min}(\omega) - \varphi_{min}(\omega_0)\right], \qquad (11)$$

where $\varphi_{min}(\omega)$ is the relative phase between the probe and the APT that minimizes the sideband intensity, $I_{2n}(\varphi_{min}(\omega)) = 0$, for $\omega = 2n\omega_R$. The subscript $final$ is used to indicate that this is the final state of the pulse as it is detected on target.

B. IN-SITU

We will now derive an analogue to Eq. 11 for the *in-situ* method, where the relative timing of the *initial* attosecond pulses is determined from the oscillation of the induced even harmonics. Using the Strong Field Approximation (SFA), the Fourier components of the HHG dipole can be approximated as [13]

$$\vec{x}_n \propto \int dt\ d\tau\ d^3\vec{p}\ \exp\left[\frac{iS(\vec{p}, t, \tau)}{\hbar} - in\omega_R t\right], \qquad (12)$$

where $\vec{p}$ is the canonical (drift) momentum, τ is the time between tunneling and recombination, S is the quasiclassical action and n is the harmonic order. Finding the stationary points of the quasiclassical action, and then applying the saddle point approximation five times reduces the integrals in Eq. 12 to a sum of discrete contributions, each corresponding to a quasiclassical trajectory [5, 14]. In the limit of a vanishing ionization potential, the quasiclassical trajectories become classical and the quasiclassical action becomes the classical action,

$$S[x(t,t')] = \int_{t-\tau(t)}^{t} dt' \left\{\frac{mv(t,t')^2}{2} + qx(t,t')E(t')\right\}, \qquad (13)$$

where x, v, m, q are the position, velocity, mass and charge of the electron respectively. We label the electron trajectories as $x = x(t,t')$, where t is the return time and t' is the integration variable for the action. The electron is released from the atom at time $t-\tau$ and accelerated by the laser field, E, until it returns and recombines with the atom at time t. In the one-color HHG, where $E = E_R = E_{R0}\sin(\omega_R t)$, the process is repeated with an alternating sign every half period, $x_R(t,t') = -x_R(t + T_R/2, t' + T_R/2)$, since $E_R(t') = -E_R(t' + T_R/2)$. The action is, however, the same $S_R(t) = S_R(t + T_R/2)$.

Adding a weak blue field, $E = E_R + E_B$, $E_B = E_{B0}\sin(2\omega_R t + \varphi)$, induces a small change of the trajectories and the accumulated action. We treat the blue field as a perturbation and expand the trajectory,

$$m\frac{d^2}{dt^2}\sum_{n=0}^{\infty}\lambda^n x^{(n)} = qE_R + \lambda qE_B, \qquad (14)$$

where λ is the usual perturbation parameter. The zeroth order solution is the same as in the one-color case, $x^{(0)} = x_R$; and the first order solution is purely given by the blue field, $x^{(1)} = x_B$. Higher orders, $n > 1$, are equal to zero. We expand the action as $S = S^{(0)} + \lambda S^{(1)} + \lambda^2 S^{(2)}$. The zeroth order action is the same as in the one-color case, $S^{(0)} = S_R$. The first order action, $S^{(1)} = \sigma$, is composed of three cross terms that can be rewritten using a few partial integrations

$$\sigma = \int_{t-\tau}^{t} dt' \left\{mv_R v_B + qx_R E_B + qx_B E_R\right\} \qquad (15)$$

$$= q\int_{t-\tau}^{t} dt'\ x_R E_B, \qquad (16)$$

where the following boundary conditions are used: $x_R(t,t) = x_R(t,t-\tau) = v_R(t,t-\tau) = x_B(t,t) = 0$. It is interesting to note that σ can be written as an integral over the unperturbed trajectory, x_R, and the blue field (or as an integral over the trajectory perturbation, x_B, and the red field). Unlike S_R, the first order action changes sign between opposite half cycles of the IR field, $\sigma(t) = -\sigma(t + T_R/2)$, which reflects the fact that the electron is now moving differently in the two half cycles, $x(t,t') \neq -x(t + T_R/2, t' + T_R/2)$. The second order action is given purely by the blue field, $S^{(2)} = S_B$, and it has, therefore, the same sign in opposite half cycles of the IR. The sum of the contributions from the zeroth and the second order is labeled as $\Sigma = S^{(0)} + S^{(2)}$.

The integrals of Eq. 12 are evaluated for the two-color case using the saddle point solutions for the IR field only,

i.e. we assume that σ and S_B are slowly varying compared to S_R. Only the two stationary points corresponding to the short branch of trajectories in two neighboring half cycles of the fundamental are used, in accordance with the experiment where the long branch has been removed using spatial filtering in a narrow aperture. It turns out that the contributions from the first order action have equal sign for the odd harmonics and opposite sign for even harmonics, which allows us to combine the terms using Euler's formula. The HHG dipole takes the following form for the odd harmonics:

$$\vec{x}_{n=2N+1} \propto \cos\left[\frac{\sigma_n}{\hbar}\right] \exp\left[\frac{i\Sigma_n}{\hbar} - in\omega_R t_n\right], \qquad (17)$$

where the first order change in action, σ_n, leads to change of dipole amplitude. In the limit of a vanishing blue field, we recover the one-color case: $\cos(\sigma_n/\hbar) \to 1$ and $\Sigma_n \to S_{Rn}$. The HHG dipole for the even harmonics takes the following form:

$$\vec{x}_{n=2N} \propto \sin\left[\frac{\sigma_n}{\hbar}\right] \exp\left[\frac{i\Sigma_n}{\hbar} - in\omega_R t_n\right], \qquad (18)$$

where the amplitude again is dependent on the change in action. The even harmonics vanish if there is no blue field since $\sin(\sigma_n/\hbar) \to 0$. The intensities of the odd and even harmonics vary out of phase: The odd harmonics decrease when the even harmonics increase. A weak blue field implies that $\sin(\sigma_n/\hbar) \approx \sigma_n/\hbar$. In this regime the even harmonic amplitudes grow linearly with the applied blue field and oscillate with the relative phase, φ. It is in this regime that an *in-situ* measurement can be carried out.

Using Eq. 16, we seek the relative phase, $\varphi_{min}(t)$, that induces no even harmonic amplitude,

$$\sigma(t, \varphi_{min}(t)) = q \int_{t-\tau(t)}^{t} dt'\ x_R(t,t') E_B(t', \varphi_{min}(t)) = 0, \qquad (19)$$

where the return time, $t = t(\omega)$, is a saddle point solution to Eq. 12 and, therefore, a function of frequency (in close analogy with Eq. 3-4). We find excellent agreement with the pioneering work of Dudovich *et. al.* [8] using unperturbed classical trajectories in Eq. 19. The solution, $\varphi_{min}(t)$, is expanded to first order around the central return time, $t_c = 0.35T_R$,

$$\varphi_{min}(t) - \varphi_{min}(t_c) \ \approx\ -(1+\xi)\ \omega_R\ (t - t_c), \qquad (20)$$

where $\xi \approx -0.06$ is the "systematic scaling difference" between φ_{min} and $\omega_R t$. Our numerical linearization of $\varphi_{min}(t)$ in Eq. 20 depends on the choice of t_c: ξ varies from 0.1 (in the shortest return) to 0 (in the cut-off regime). It is, however, the scaling around the central return time (central frequency) that is most appropriate for calculating the initial properties of the entire attosecond pulse. Using Eq. 8 and Eq. 20, we find the following simple relation between the oscillations in the even harmonics and the relative emission time from the atom

$$t^{(rel)}_{initial}(\omega, \omega_c) \approx -\frac{\gamma}{\omega_R}\ \left[\varphi_{min}(t(\omega)) - \varphi_{min}(t(\omega_c))\right], \qquad (21)$$

where $\gamma = 1/(1+\xi) \approx 1.06$ is a correction factor. Eq. 21 resembles Eq. 11 from the RABITT section in both form and interpretation. The even harmonic oscillations are mapping out the relative emission times from the atom much like the sidebands in a RABITT scan map out the relative arrival times on target. In contrast to RABITT, the *in-situ* method needs a correction factor, γ, which is slightly larger than one for the short branch of trajectories. The validity of Eq. 21 is limited to the high-order harmonic plateau where the constant amplitude approximation [Eq. 12] and the linearization of $\varphi_{min}(t)$ [Eq. 20] are sound. The *in-situ* method can be applied also to the second (long) branch of trajectories. The correction factor for the long branch is $\gamma \approx 0.88$ for $t_c = 0.55T_R$.

We want to stress that the *in-situ* method is *not* a direct measure of the emission time (or the group delay), because $\varphi_{min}(t)$ is not related to the return time in a trivial way [Eq. 19]. In fact, one could also interpret the *in-situ* method as a measurement of the continuum time which is an equally good parameter of the process.

All technical details aside, we have found that the *in-situ* method produces traces of oscillating even harmonics which, to reasonable agreement, can be treated as RABITT scans. In the following, we will present data which is uncorrected, $\gamma = 1$, verifying numerically and experimentally the validity of $\gamma \approx 1$ for harmonics in the plateau. Unlike RABITT, the *in-situ* method is not limited to sampling the relative timing at only even harmonic energies. The oscillations in the odd harmonic energies [Eq. 17] can be treated in a similar way, thus doubling the number of sampling points for the relative timing compared to RABITT.

C. Numerical SFA calculation

We perform a numerical experiment using SFA to verify the analytical work presented in the previous subsection for an IR intensity of $I_R = 2 \times 10^{14}$ W/cm^2. Our numerical calculations are based on Eq. 13 in [5] where the saddle point approximation is done only over $\vec{p}$ space. The integration over continuum time, τ, and actual time, t, is done numerically. This allows us, in a simple way, to access either branch of trajectories by numerically restricting the integral over the continuum time, τ. We calculate the single atom response for the short branch of trajectories by restricting the continuum time integral to $0 < \tau < 0.65T_R$. Then we calculate the response from the long branch of trajectories by restricting the continuum time integral to $0.65T_R < \tau < T_R$. The corresponding group delays are calculated numerically from the first derivative of the spectral phase of the short branch dipole [Fig. 3(a) $\circ$] and the long branch dipole [Fig. 3(a) $\bullet$].

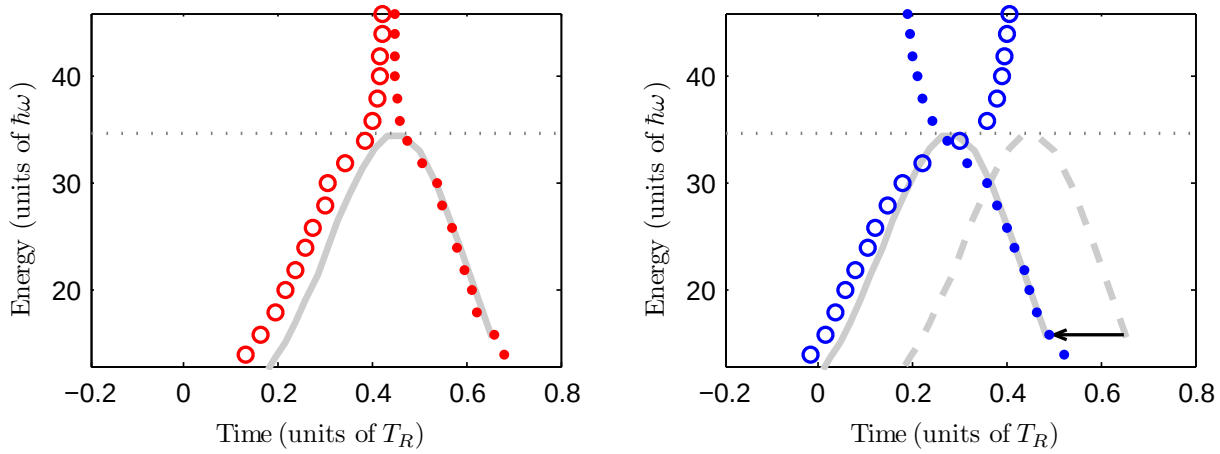

FIG. 3: (Color online) (a) The single atom response of the short (○) and the long (●) branches are calculated using SFA for a typical IR intensity, $I_R = 2\times10^{14}$ W/cm^2. The group delays, $-d\phi/d\omega$, of both branches are in good agreement with the simple classical model (gray line). The group delay branches merge beyond the cut-off (dotted line). (b) The numerical *in-situ* scans generated using SFA with a weak blue field, $I_B/I_R = 0.1\%$, show qualitative agreement for both the short (○) and the long (●) branch with the shifted simple classical model (gray line). The *in-situ* branches do not merge beyond the cut-off (dotted gray line).

The time-energy curves are compared to a simple classical model [Fig. 3(a) gray line], consisting in finding the classical kinetic return energy for a classical electron in a sinusoidal electric field, $E(t) = E_0 \sin\omega t$, which starts and returns to the origin, and then adding the ionization energy.

Next, we perform the numerical *in-situ* measurement by calculating the single atom response from the same IR field plus a weak blue field with a relative intensity of $I_B/I_R = 0.1\%$. The phase of the blue field, φ, is then shifted relative to the IR and the atomic response is calculated again. As expected, we obtain weak oscillations in the even harmonics which vary with respect to φ. The relative phases, φ_{min}, that minimize the even harmonic signal are extracted from the short branch [Fig. 3(b) ○] and the long branch [Fig. 3(b) ●]. We find that the *in-situ* method produces time-energy slopes that are in qualitative agreement with a shifted simple classical model [Fig. 3(b) gray line] for harmonics below the cut-off [Fig. 3(b) dotted line]. There is, however, an absolute time difference between the delays that minimize the even harmonic signal, $-\varphi_{min}/\omega_R$, and the (unshifted) simple classical model [Fig. 3(b) dashed gray line]. A careful study of the numerical experiment indicates that the *in-situ* measurement suffers from a small systematic deviations from the group delay which can be attributed to the correction factor, γ. We stress that all data presented in Fig. 3(b) is uncorrected, *i.e.* $\gamma = 1$.

A larger, and possibly more interesting, systematic deviation between the group delay and the *in-situ* method arises for harmonics close to and beyond the cut-off [Fig. 3(a)-3(b) dotted line]. This deviation occurs in a spectral region where Eq. 3-4 are questionable and it is, therefore, more difficult to interpret the deviation. It is clear, however, that the *in-situ* measurement is not a direct measurement of the group delay (nor the relative timing) of the attosecond pulses and that a deeper analysis is needed for understanding the behavior beyond the cut-off. It is interesting to note that the *in-situ* measurements of the short branch and of the long branch do not merge in the cut-off. We verify that the strange cut-off behavior is not an artifact of the trajectory separation by calculating the combined response of the short and the long branch, $0 < \tau < T_R$. The *in-situ* measurement of the combined branches results in a chaotic behavior in the plateau region due to interferences between the two branches; and a steady solution in the cut-off region that tends toward the long branch. Our interpretation, of this numerical experiment, is that the dominant physical contribution comes the long branch beyond the cut-off. The dominance of the long branch beyond the cut-off region has been stressed by Lewenstein *et. al.* [15], but it has never been demonstrated experimentally.

The numerical experiment is repeated at progressively higher relative intensities to investigate the robustness of the *in-situ* method. We observe the depletion of the odd harmonics, as expected from Eq. 17. The information retrieved from the even harmonics is intact as long as $I_B/I_R < 1\%$ for $I_R = 2\times10^{14}$ W/cm^2. Increasing the relative intensity further results in an invalid *in-situ* measurement.

III. EXPERIMENTAL SETUP

The experimental work is carried out at the Lund Laser Center (LLC) using a kHz Ti-Sapphire chirped pulse am-

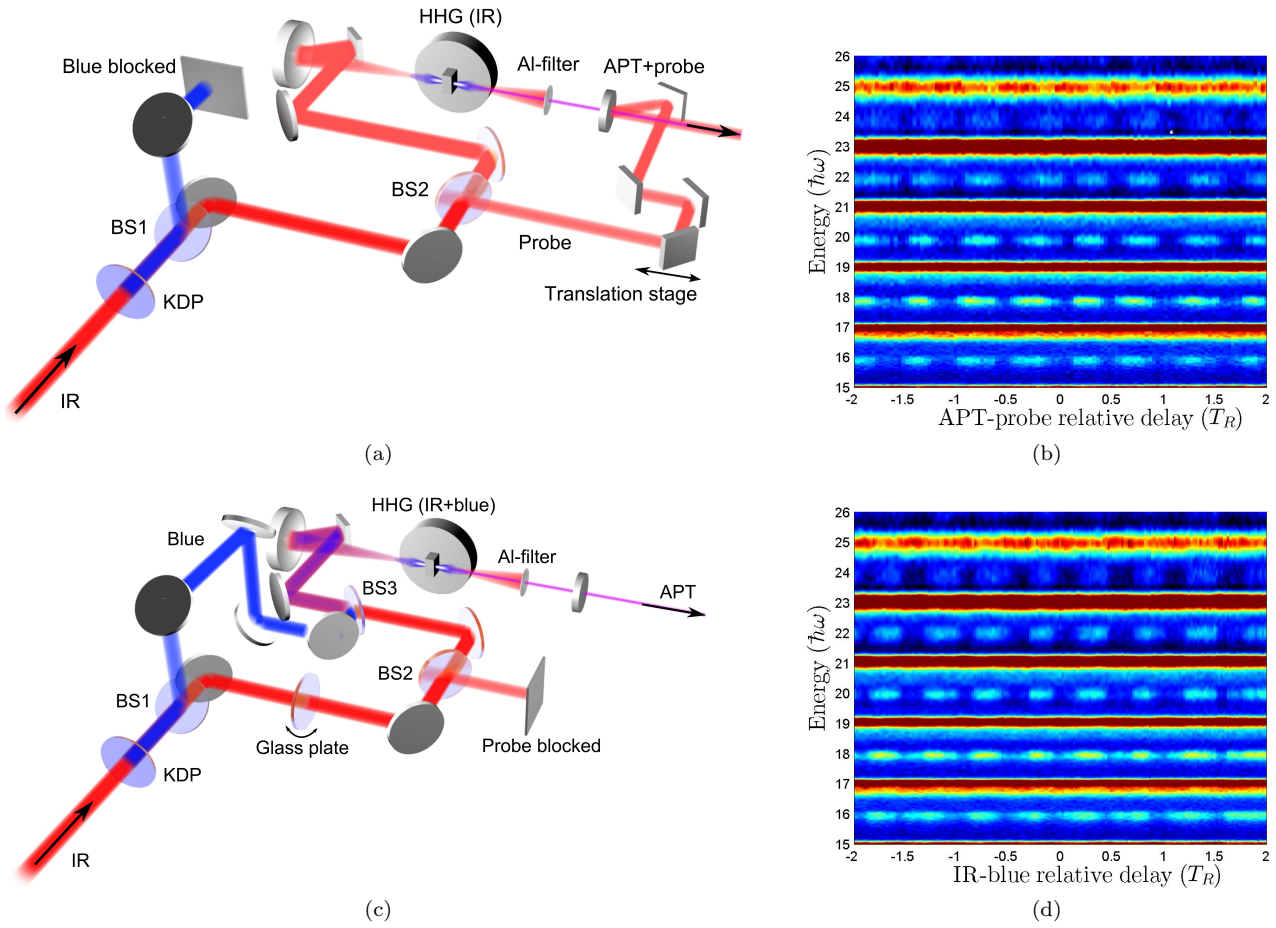

FIG. 4: (Color online) (a) In RABITT mode the blue field [from KPD] is split off [BS1] and blocked. A weak IR probe field is created [BS2] and delayed on the subcycle scale using a translation stage. The APT is generated from the intense IR pulses [HHG (IR)] in a synchronized pulsed gas cell. The intense IR field is eliminated using aluminum filter(s). The APT and the probe are recombined [APT+probe] using a mirror with a narrow aperture. The APT passes through the aperture while the probe is reflected on the mirror. The temporally overlapping APT and probe field are then focused using a toroidal mirror and detected using an electron spectrometer [not shown]. (b) The RABITT scan is recorded using an electron spectrometer with subcycle synchronization of the APT and the probe in the detection chamber. (c) In *in-situ* mode the IR and the blue field [from KDP] are separated [BS1] into a dichroic interferometer. The IR field is delayed on the subcycle scale using a glass plate (which can be tilted) before it is recombined with the blue field [BS3]. The probe is blocked [after BS2]. The APT is generated from intense IR pulses in the presence of a weak blue field [HHG (IR+blue)] in a synchronized pulsed gas cell. The IR and blue fields are eliminated using aluminum filter(s). The APT is detected using an electron spectrometer [not shown] after passing a narrow aperture. (d) The *in-situ* scan is recorded using an electron spectrometer with subcycle synchronization of the IR and the blue fields in the generation cell [HHG (IR+blue)]. The colorscale in (b) and (d) is saturated so that the interferometric beating is more clearly seen.

plified laser operating at a wavelength of 800 nm (IR). The pulse energy is 2 mJ and the pulse length is 35 fs. The APTs are generated by focusing the IR laser pulses into a synchronized pulsed argon gas cell [16]. Having a pulsed gas cell allows us to maintain a low average background pressure in the generation chamber while the effective gas pressure in the gas cell is high. We do not measure the instantaneous generation pressure in the gas cell but it is reasonable to assume that it scales with the average background pressure in the generation chamber.

We use aluminum filters after the HHG to:

- Remove the remaining IR and the low-order harmonics in the pump line
- Compress the pulses in the APT

Eliminating the intense IR beam after the generation cell is important since neither of the characterization schemes work if there is a strong IR field present in the detection process. The individual filters are 200 nm thick and the number of filters used can be changed using a motorized filter holder [6]. Being able to change the number of filters is important in order to access the effect of filters on the attosecond pulses [3]. The attosecond pulses are finally detected using a magnetic bottle electron spectrom-

eter (MBES). The detection gas is Argon which allows us to study the high-order harmonics from the plateau and cut-off regions.

In the RABITT method the ionization step in the MBES is perturbed by a synchronized weak IR probe field, which is coupled into the MBES using a Mach-Zehnder interferometer [Fig. 4(a)]. The relative phase, φ, between the APT and the IR is controlled using a piezo-electric translation stage in the interferometer. A typical RABITT scan is shown in Fig. 4(b).

In the *in-situ* method the IR pulse is used to generate a second harmonic field (blue) with a 1.3 mm thick KDP type I crystal. The IR and the blue field are synchronized before the generation chamber using a three dimensional dichroic interferometer [Fig. 4(c)]. A glass plate in the interferometer enables control of the relative phase, φ, between the IR and the blue fields. The interferometer is engineered so that the polarizations of the recombined red and blue fields are parallel [17]. A typical *in-situ* scan is shown in Fig. 4(d). Using Eq. 11 and Eq. 21, we know that the information about the attosecond pulses is derived in the same way from both methods, while the physical interpretation of the two measurements differs.

IV. PROOF OF PRINCIPLE FOR *IN-SITU* MEASUREMENTS

In this section, we study the properties of an APT using both the RABITT and the *in-situ* method. A direct comparison of the two measurements is not meaningful since attosecond pulses are probed at different times. Two main effects influence the properties of the attosecond pulses:

- Dispersion from the Al filters
- Phase matching in the generation cell

To avoid effects due to phase matching as much as possible [2, 21], we perform the measurement at the lowest possible pressure, corresponding to a background pressure of $P_G \approx 1.5$ μbar. At this pressure, the high-order harmonic signal is weak but still stable enough for both characterization methods to work. The results from the RABITT method are shown in Fig. 5(a) and the results from the *in-situ* method are shown in Fig. 5(b).

The change in relative timing induced to an attosecond pulse propagating through one aluminum filter, $\Delta t_{Al}^{(rel)}(\omega, \omega_0)$, can be determined using two RABITT measurements,

$$\Delta t_{Al}^{(rel)}(\omega) = t_{final_2}^{(rel)}(\omega) - t_{final_1}^{(rel)}(\omega), \tag{22}$$

where $t_{final_1}^{(rel)}$ is the relative timing of the attosecond pulse having passed one filter and $t_{final_2}^{(rel)}$ is the relative timing after passing two filters. Note that we now drop the notation for the reference frequency since it is $\omega_0 = 14\omega_R$ for all experimental data. We have verified that $\Delta t_{Al}^{(rel)}(\omega)$ agrees with the GD deduced from the refractive index of aluminum [18]. Assuming that the two filters are identical we can calculate the relative timing of the attosecond pulse before passing the filter(s),

$$t_{final_0}^{(rel)}(\omega) = t_{final_1}^{(rel)}(\omega) - \Delta t_{Al}^{(rel)}(\omega). \tag{23}$$

The "unfiltered" relative timing of attosecond pulses [Fig. 5(a) ∘] is in good agreement with the simple classical model [gray line] for an effective intensity of $I_R \approx 1\times10^{14}$ W/cm^2. This intensity corresponds to a cut-off at harmonic 23, which agrees well with spectral measurements taken without the probe field present.

Having estimated the initial state of the attosecond pulses using the RABITT method, we now proceed with the *in-situ* scheme. One important advantage of the *in-situ* scheme is that all information is imprinted spectrally, which makes it possible to analyse attosecond processes with great accuracy using a photon spectrometer rather than an electron spectrometer. In this paper, however, we use the same MBES as for the RABITT so that a straightforward comparison of the two schemes is made.

The *in-situ* measurements are taken immediately after their respective RABITT measurements for one and two aluminum filters [Fig. 5(b)]. The HHG conditions, therefore, have little time to evolve when changing schemes (a few seconds). The filters should not influence the *in-situ* measurement because the information is imprinted spectrally already in the HHG process. Using the *in-situ* scheme, we should ideally obtain identical information regardless of the number of filters. The measurements again nicely follow the classical model for $I = 1 \times 10^{14}$ W/cm^2 [gray curve]. We determine the initial relative timing, $t_{initial}^{(rel)}(\omega)$, and compare it to the relative timing obtained with the RABITT method, $t_{final_0}^{(rel)}(\omega)$, in Fig. 5(c). The corresponding GDD is calculated by fitting a line to the relative timing using sidebands/even harmonics 14 to 22

$$-\left.\frac{d^2\phi}{d\omega^2}\right|_{18\omega_R} \approx \begin{cases} 2.31 \times 10^4 \text{ as}^2/\text{rad} & \text{(RABITT)} \\ \gamma \times 2.24 \times 10^4 \text{ as}^2/\text{rad} & (\textit{in-situ}), \end{cases} \tag{24}$$

with a root mean square (RMS) deviation of approximately 23 as for the corresponding difference in relative timing. We treat the *in-situ* data as a RABITT scan, and the numerical value of the GDD must, therefore, be multiplied by the correction factor, γ. The experiment shows that the correction factor is close to unity for the short branch, as expected from the theory section. The good agreement between these measurements shows that the either the RABITT or the *in-situ* method can be used to characterize the APTs at low generation pressures for energies in the central and upper region of the harmonic plateau.

It is tempting to increase the intensity of the blue field so that the even harmonics become stronger and more visible. We use an adjustable aperture in the blue arm of the three dimensional dichroic interferom-

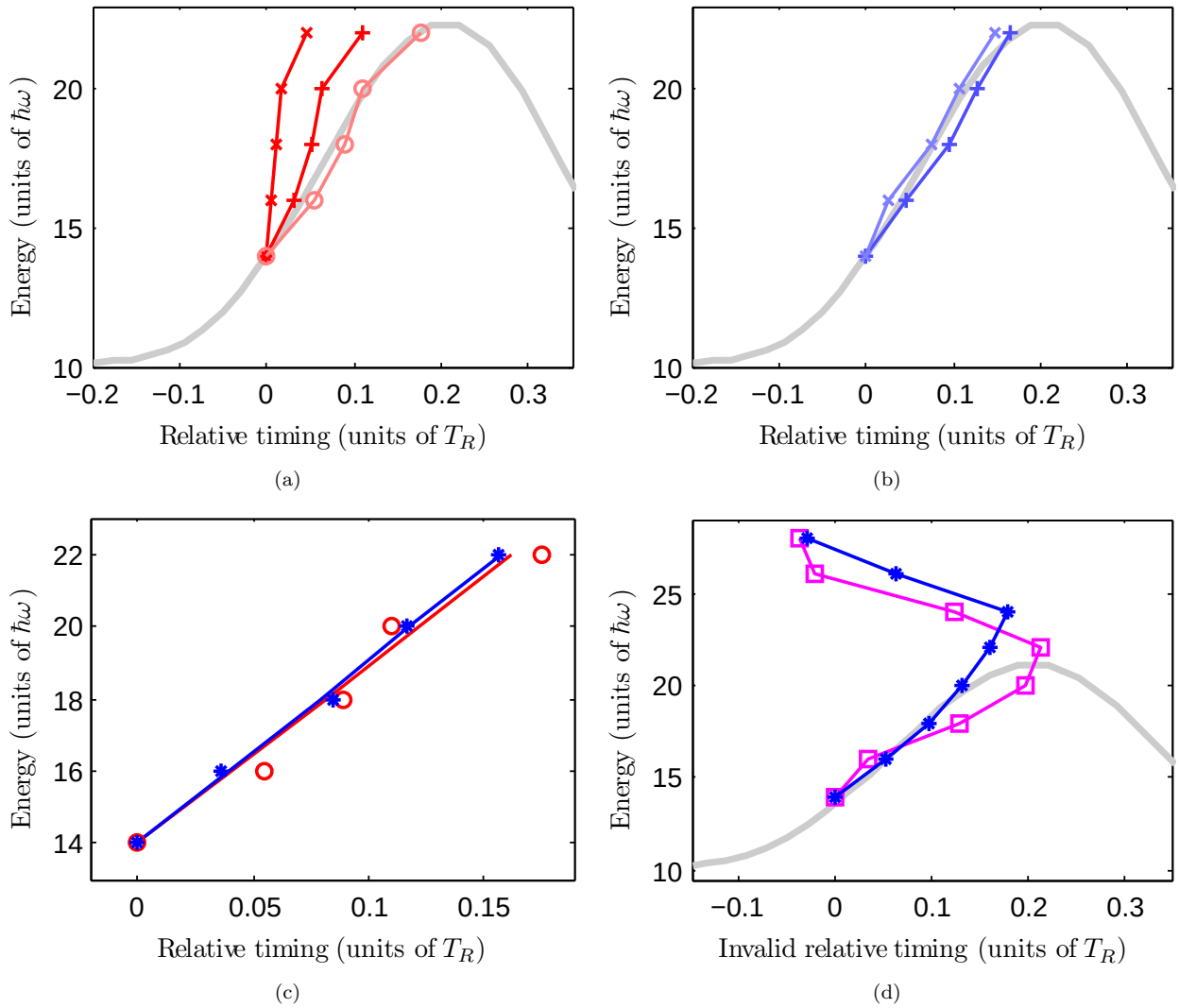

FIG. 5: (Color online) (a) RABITT measurements with one (+) and two (×) aluminum filters are used to determine the relative timing of the unfiltered attosecond pulses (○). All temporal measurements are presented as relative timings with reference to harmonic 14. (b) *In-situ* measurements with one (+) and two (×) aluminum filters. The data is uncorrected, $\gamma = 1$. The simple classical model ($I_R = 1 \times 10^{14}$ W/cm^2) [5(a)-5(b) gray curve] is plotted for reference. (c) Unfiltered RABITT measurement (red ○) compared to the average *in-situ* measurement (blue ∗). (d) A slight increase of the blue intensity (blue ∗) has a small effect on the measurement in the harmonic plateau (harmonic $14 - 24$). Increasing the blue intensity further (pink □) results in an invalid measurement. The simple classical model ($I_R = 0.9 \times 10^{14}$ W/cm^2) [gray line] is plotted for reference. Beyond the cut-off (harmonic $24 - 28$), a similar shift occurs as for the long branch in Fig. 3(b).

eter so that the intensity of the blue field can be increased while all other experimental parameters are constant. It has been demonstrated that an increased blue intensity will alter the quasiclassical trajectories in the HHG process [19, 20], but a systematic study of how the *in-situ* method breaks down has not yet been reported. Even harmonic oscillations appear *beyond the cut-off* for a slight increase of the blue intensity. The information extracted from these oscillations show strong deviations with the expected group delays, while the information from the plateau region remains rather accurate [Fig. 5(d) ∗]. Even harmonic oscillation beyond the cut-off regime should, therefore, *not* be included in our simple interpretation [Eq. 21] of the *in-situ* method. The experimental results beyond the cut-off are in qualitative agreement with the numerical calculations shown in Fig. 3(b), which indicates that it is the long branch of trajectories that contribute to the cut-off regime. At moderately higher blue intensities we observe a shift of the modulations in the plateau [Fig. 5(d) □]. This shows that the *in-situ* method now predicts the wrong relative timing for the initial attosecond pulses also in the plateau region and that the relative intensity must be reduced.

V. COMPARISON OF RABITT AND *IN-SITU* MEASUREMENTS AT HIGHER PRESSURE

We now study how the phase of the attosecond pulses is modified due to a higher gas pressure in the generation chamber. It has recently been shown that in some conditions an increasing gas pressure can lead to a compression of the attosecond pulses [21]. The effect predicted theoretically was, however, small and difficult to demonstrate experimentally. Here, combined measurements using the RABITT and the *in-situ* method allows us to unambiguously extract the contribution of phase matching to the temporal structure of attosecond pulses.

RABITT results obtained at different pressures are shown in Fig. 6(a). The data is collected with one aluminum filter, but the effect of this filter is removed using Eq. 23. The corresponding *in-situ* measurements are shown in Fig. 6(b). The *in-situ* measurements are mostly insensitive to the increased gas pressure, while the RABITT measurements are deformed in a nontrivial way. Deviations in relative timing for attosecond pulses due to the macroscopic propagation through the gas cell can be extracted by subtracting the final and initial relative timings

$$\Delta t^{(rel)}_{macro}(\omega, P_G) = t^{(rel)}_{final_0}(\omega, P_G) - t^{(rel)}_{initial}(\omega, P_G), \quad (25)$$

where we have explicitly written P_G to indicate that the macroscopic effects depends on the gas pressure. In $t^{(rel)}_{initial}(\omega, P_G)$, the P_G dependence refers to a possible change of the fundamental field in the nonlinear medium that could affect the single atom response. The results are shown in Fig. 6(c), together with the effect of a 200 nm-Al filter (gray). Macroscopic effects introduce a (non-trivial) negative relative timing, first decreasing then increasing with frequency. The corresponding induced GDD might help to compensate for the single atom GDD for low orders, but for higher orders the GDD is increased. These results agree well with those presented in [21].

To understand the origin of the macroscopic group delay, we perform a simple model calculation [21, 22]. We consider for simplicity a one-dimensional approximation, along the propagation axis, z; a homogeneous medium of length L and a collimated geometry. In this simple case, the contribution of the single atom response and of propagation can be separated and the effect of propagation both on the phase (or more exactly phase variation) and amplitude of the nth harmonic can be described by

$$F_n = \frac{1 - \exp\left[(-i\Delta k_n - \kappa_n)L\right]}{i\Delta k_n + \kappa_n} = |F_n| \exp\left[i\phi^{mac}_n\right]. \quad (26)$$

The phase mismatch Δk_n is equal to $k_n - nk_1$, where k_n and k_1 denote the wave vector of harmonic n and the fundamental respectively. Absorption at the nth harmonic frequency is described by κ_n. The macroscopic phase can be written as

$$\phi^{mac}_n = -\arctan\left[\frac{\sin[\Delta k_n L]}{\cos[\Delta k_n L] - \exp[\kappa_n L]}\right] - \arctan\left[\frac{\Delta k_n}{\kappa_n}\right]. \quad (27)$$

Fig. 6(d) presents in color its derivative as a function of harmonic order and pressure. These results show a variation of the phase derivative that qualitatively agrees with the measured one. For a given pressure > 20 mbar, the induced GD is negative, showing a decrease at low orders, a minimum around the 23rd harmonic, followed by an increase. We stress that this satisfactory agreement is obtained with a simple model, not including the geometric phase due to focusing or two-dimensional effects. Combined RABITT and *in-situ* measurements provide a way to really unravel the effect of propagation in the generation of attosecond pulses.

VI. CONCLUSIONS

We have performed a proof of principle experiment for the *in-situ* scheme, by comparing it to the well established RABITT method. We have found excellent agreement between the methods at low generation gas pressures when the macroscopic phase matching plays a negligible role.

We have found that it is *not* possible to use the *in-situ* scheme to predict the final relative timing of the average attosecond pulses if the generation pressure is high or if it passes through some unknown dispersive material. It is equally important to realize that accurate single atom measurements can not be conducted at high generation gas pressures with the RABITT scheme. In a RABITT measurement there will always be a trade off between the number of XUV photons generated and their phase perturbation from propagation through the generation cell.

The advantages and disadvantages of the two schemes become quite clear when the generation pressure is high and one could argue that *both* schemes are needed for a more complete understanding of the attosecond pulse production and propagation.

Acknowledgments

This research was supported by the Marie Curie Early Stage Training Site MAXLAS, the Marie Curie Individual European Fellowship ATTOCO, the European Research Council (ALMA), the Swedish Research Council, in particular through the LLC Linneaus grant and the Knut and Alice Wallenberg Foundation.

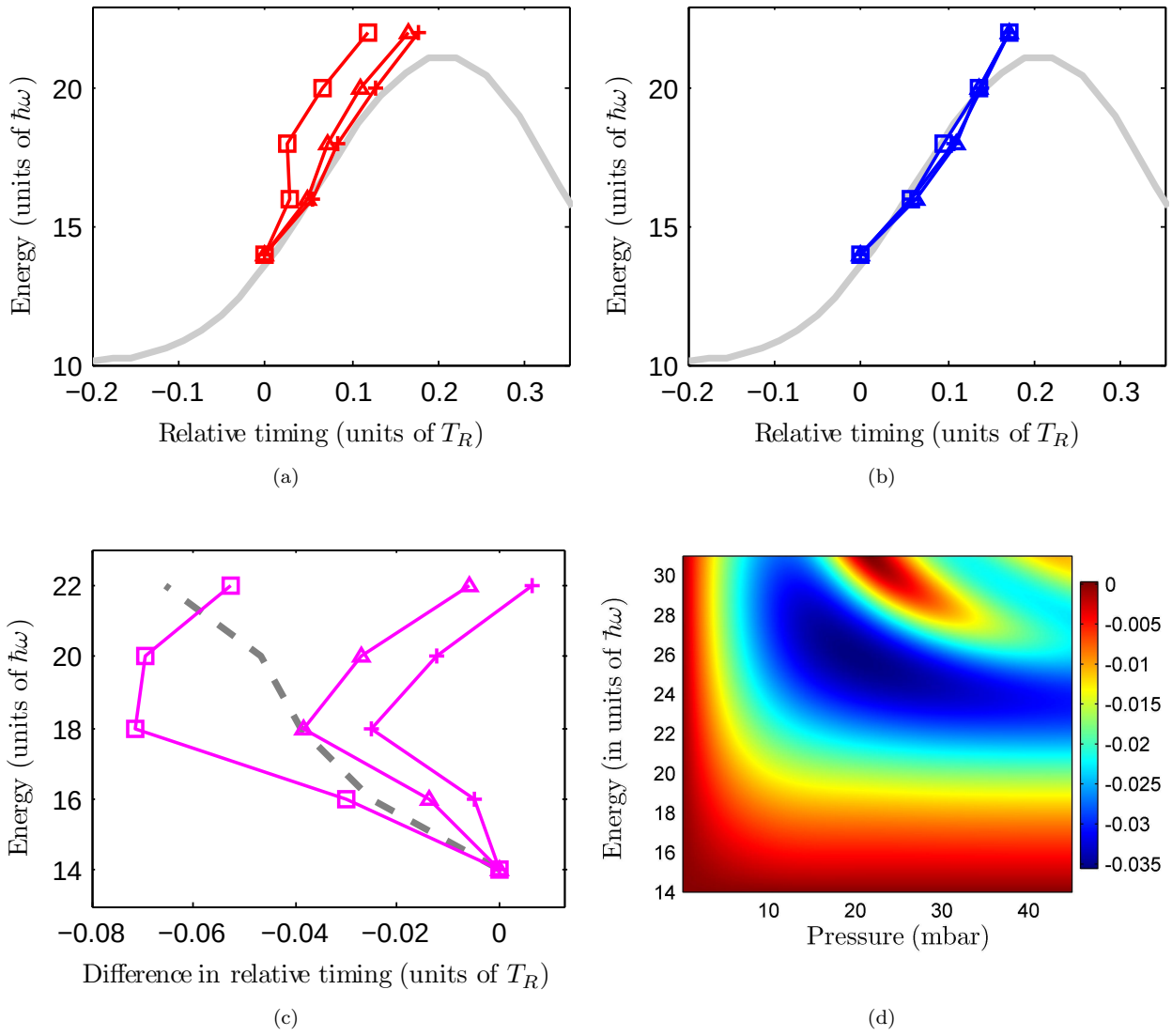

FIG. 6: (Color online) (a) Relative timing measurements from RABITT for a variety of high background pressures in the generation chamber: 5×10^{-3} (×), 6×10^{-3} (△) and 7×10^{-3} (□) mbar (the exact instantaneous pressure in the gas cell is unknown). The effect of the Al-filter has been subtracted. At high pressures there is an increased deviation from the simple classical model ($I_R = 0.9 \times 10^{14}$ W/cm^2) [gray curve]. (b) The corresponding *in-situ* measurements are mostly unaffected by the increased pressure. The data is not corrected, $\gamma = 1$. (c) The difference in relative timing, $\Delta t^{(rel)}_{macro}(\omega, P_G)$, (pink ×, △, □) is interpreted as the macroscopic delay due to phase matching in the gas cell. The symbols correspond to the same pressures as in the figures above. The delay from phase matching has approximately the same magnitude as an aluminum filter [gray dashed curve]. (d) The relative timing due to phase matching [false color in units of T_R] is calculated using a one dimensional model [21] for pressures ranging from 0 to 100 mbar. The intensity used in the model is 1.25×10^{14} W/cm^{-2}; and the duration of the pulse is 35 fs. The length of the cell is modeled as 5 mm.

References

[1] P. M. Paul *et al.*, Science **292**, 1689 (2001).
[2] M. B. Gaarde, J. L. Tate, and K. J. Schafer, J. Phys. B **41**, 132001 (2008).
[3] R. López-Martens *et al.*, Phys. Rev. Lett. **94**, 033001 (2005).
[4] Y. Mairesse *et al.*, Science **302**, 1540 (2003).
[5] M. Lewenstein *et al.*, Phys. Rev. A **49**, 2117 (1994).
[6] E. Gustafsson *et al.*, Optics Letters **32**, 1353 (2007).
[7] A.-S. Morlens *et al.*, Opt. Lett. **31**, 1558 (2006).
[8] N. Dudovich *et al.*, Nature Phys. **2**, 781 (2006).
[9] J. Itatani *et al.*, Nature **432**, 867 (2004).
[10] Even harmonics are not generated if there is no blue field present due to parity conservation.
[11] J. Mauritsson, M. B. Gaarde, and K. J. Schafer, Phys.

Rev. A **72**, 013401 (2005).
[12] Except for the carrier envelope phase of the attosecond pulse.
[13] M. Lewenstein, P. Salières, and A. L'Huillier, Phys. Rev. A **52**, 4747 (1995).
[14] P. Salières *et al.*, Science **292**, 902 (2001).
[15] M. Lewenstein *et al.*, Phys. Rev. A **51**, 1495 (1995).
[16] E. Gustafsson and T. Ruchon, Lund Reports on Atomic Physics **366**, (2006).
[17] J. Mauritsson, J. M. Dahlström and T. Fordell, Accepted for publication in J. Phys. B.
[18] O. E. Martinez, J. P. Gordon, and R. L. Fork, J. Opt. Soc. Am. B **1**, 1003 (1984).
[19] J. Mauritsson *et al.*, Phys. Rev. Lett. **97**, 013001 (2006).
[20] E. Mansten *et al.*, New. J. Phys. **10 No.8**, 083041 (2008).
[21] T. Ruchon *et al.*, New. J. Phys. **10 No. 2**, 025027 (2008).
[22] E. Constant *et al.*, Phys. Rev. Lett. **82**, 1668 (1999).